Received: 29 June 2019 | Revised: 28 October 2019 | Accepted: 3 November 2019

DOI: 10.1111/avsc.12466

RESEARCH ARTICLE

Applied Vegetation Science IAVS

Detecting changes in understorey and canopy vegetation cycles in West Central Alberta using a fusion of Landsat and MODIS

Cameron J. R. McClelland[1] | Nicholas C. Coops[1] | Ethan E. Berman[1] | Sean P. Kearney[1] | Scott E. Nielsen[2] | A. Cole Burton[3] | Gordon B. Stenhouse[4]

[1]Integrated Remote Sensing Studio (IRSS), Department of Forest Resource Management, University of British Columbia, Vancouver, BC, Canada

[2]Applied Conservation Ecology Lab, Department of Renewable Resources, Faculty of Agriculture, Life, and Environmental Sciences, University of Alberta, Edmonton, AB, Canada

[3]Wildlife Coexistence Lab, Department of Forest Resource Management, University of British Columbia, Vancouver, BC, Canada

[4]fRI Research, Hinton, AB, Canada

Correspondence
Cameron J. R. McClelland, Integrated Remote Sensing Studio (IRSS), Department of Forest Resource Management, 2424 Main Mall, University of British Columbia, Vancouver, BC, V6T 1Z4, Canada.
Email: cammcclell@gmail.com

Funding information
Grizzly-PAW Project, Grant/Award Number: 486175-15; Shell; University of British Columbia

Co-ordinating Editor: Duccio Rocchini

Abstract

Aims: To model regional vegetation cycles through data fusion methods for creating a 30-m daily vegetation product from 2000 to 2018 and to analyze annual vegetation trends over this time period.

Location: The Yellowhead Bear Management Area, a 31,180-km^2 area in west central Alberta, Canada.

Methods: In this paper, we use Dynamic Time Warping (DTW) as a data fusion technique to combine Landsat 5, 7 and 8 satellite data and Moderate Resolution Image Spectroradiometer (MODIS) Aqua and Terra imagery, to quantify daily vegetation using Enhanced Vegetation Index at a 30-m resolution, for the years 2000–2018. We validated this approach, entitled DRIVE (Daily Remote Inference of VEgetation), using imagery acquired from a network of ground cameras.

Results: When DRIVE was compared to start and end of season dates (SOS and EOS respectively) derived from ground cameras, correlations were r = 0.73 at SOS and r = 0.85 at EOS with a mean absolute error of 7.17 days at SOS and 10.76 days at EOS. Results showed that DRIVE accurately increased spatial and temporal resolution of remote-sensing data. We demonstrated that SOS is advancing at a maximum rate of 0.78 days per year temporally over the 18-year time period for varying elevation gradients and land cover classes over the region.

Conclusions: With DRIVE, we demonstrate the utility of DTW in quantifying vegetation cycles over a large heterogeneous region and determining how changing climate is affecting regional vegetation. DRIVE may prove to be an important method to determine how carbon sequestration is varying within fine-scale individual plant communities in response to changing climate and likely will be beneficial to wildlife movement and habitat selection studies examining the varying response of wildlife species to changing vegetation cycles under shifting climatic conditions.

KEYWORDS

30-m resolution, daily remote inference of vegetation, DRIVE, dynamic time warping, fusion, Landsat, MODIS, remote sensing, time series, vegetation cycles

1 | INTRODUCTION

1.1 | Ecological importance of vegetation events

The timing and distribution of recurring events in vegetation dynamics, such as green-up, flowering, fruiting and senescence, are bottom-up drivers for many ecosystem processes. The development of vegetative food resources which occur on a landscape seasonally, and annually, have been shown to be key drivers for wildlife movement and habitat selection (Nijland et al., 2013), while monitoring the variations of vegetation cycles has provided a basis to define the progression of climate change (Brown et al., 2016). Furthermore, carbon sequestration in vegetation is known to be influenced positively by growing season length (Keenan et al., 2014). The timing of vegetative cycles is essential in determining how vegetation is changing seasonally and annually; however, a lack of precise information on the timing and spatial distribution of vegetative events currently limits our ability to incorporate vegetative cycles into ecological and climatic modelling.

Vegetative cycles are complex and species-specific (Uemura, 1994), driven by regional climate variables, such as temperature and precipitation, coupled with localized processes such as snowmelt and overstorey structures (Nijland, Bolton, Coops, & Stenhouse, 2016). Climate change is affecting canopy and understorey vegetation cycles and timing of key events such as green-up and senescence of vegetation (Beaubien & Hamann, 2011) and conceivably in different ways with canopy vegetation cycles potentially being disconnected to the understorey species due to variations in temperature, and growing season length and moisture availability. Average start of the growing season has shifted globally; for example, in the boreal forest, an advancement of green-up by 2–14 days per decade has been reported (Delbart et al., 2008; Ma, Pitman, Lorenz, Kala, & Srbinovsky, 2016). Trophic mismatches — where the timing of repeated life cycle phases for interacting species are changing at different rates — are occurring due to climate change and across many species including, plants, birds, mammals and insects (Renner & Zohner, 2018). For example, roe deer across Europe rely on timing birth with green-up to take advantage of the entire growing season. Green-up and birthing events are becoming misaligned as green-up is beginning earlier, creating a trophic mismatch where newborns are not able to acquire as much nutrition, reducing their survival rates (Plard et al., 2014). In western Canada, with the changing climate, berry ripening is occurring earlier and creating a potential trophic mismatch that would require grizzly bears (*Ursus arctos*), who rely heavily on berries for hibernation, to obtain nutrition from other sources prior to den entry (Laskin, 2017). In order to derive annual and seasonal vegetation patterns, and facilitate predictive models of climate change and wildlife habitat selection and movement patterns, vegetation must first be quantified at a regional scale and with a fine spatial and temporal resolution.

1.2 | Remote monitoring of vegetation events

Changes in green-up and senescence of vegetation can be monitored using a variety of techniques at a range of spatial scales. Ground-based field surveys are the most common and for which the longest historical data archive is available (Schwartz, 2003). This involves establishing permanent plots and revisiting them at set intervals to record the vegetative and reproductive phase of plants. This technique has been widely used throughout Europe, Asia and North America (Beaubien & Hamann, 2011), and in some cases, historical records exist dating back centuries (European Phenology Record) or even a millennium (Kyoto cherry blossom records; Aono & Kazui, 2008). With ground-based observations, vegetation data are gathered at fine spatial scales; however, observations are limited to present species at discrete points in time (often with large temporal gaps) and for individual point locations. Therefore, it is difficult to gain landscape perspectives (White, Hoffman, Hargrove, & Nemani, 2005).

Recording of vegetation phases using time-lapse photography allows researchers to obtain vegetation changes at a fine temporal resolution with comparable spatial scales to ground-based field observations. It also allows objective capture of vegetation phases that can be analyzed visually by users or by automatic algorithms. Networks of cameras can be established on a seasonal (Nijland et al., 2013) or permanent basis (The Phenocam Network) (Richardson et al., 2018) and have been shown to be useful for tracking green-up and senescence of key vegetative food species (Bater et al., 2011; Laskin, 2016; Nijland et al., 2013). Despite its high temporal resolution and accuracy, time-lapse photography still lacks the spatially explicit information to measure vegetation cycles continuously in space and time.

Satellite-based remote-sensing techniques have been used intensively for the past three decades to describe vegetation cycles spatially by means of dense temporal spectral vegetation indices. Indices such as the normalized difference vegetation index (NDVI) and the Enhanced Vegetation Index (EVI) incorporate reflectance of the visible and near-infrared portions of the electromagnetic spectrum to monitor vegetation (Huete, Mustard, & Vadeboncoeur, 2006). Space-borne sensors enable the monitoring of vegetation data across broad spatial scales and are able to acquire data for remote regions inaccessible to ground-based methods (Zhang et al., 2003). While these sensors typically cannot achieve the same fine spatial (species level) resolution possible with ground or camera-based techniques, data can be combined with those from cameras to validate and exploit the key benefits of the two complementary approaches (Melaas, Friedl, & Zhu, 2013).

One of the most commonly used sensors is the Moderate Resolution Image Spectroradiometer (MODIS). For example, Beck, Atzberger, Høgda, Johansen, and Skidmore (2006) used daily NDVI derived from MODIS at 250-m spatial resolution to fit a time series using a double logistic function to model high-latitude vegetation cycles in northern Scandinavia. Soudani et al. (2008) used MODIS 250-m EVI time series data fit to a double sigmoid function to model vegetation transition dates in comparison to ground camera data in French deciduous forests. While accurate at broad spatial scales

when comparing MODIS to observed vegetation trends, a reoccurring challenge using MODIS observations is the lack of fine-scale spatial resolution, resulting in a failure to resolve small-scale variation in heterogeneous landscapes (Coops et al., 2012; Hufkens et al., 2012).

The launch of Landsat with the Thematic Mapper™ instrument in 1984 allowed production of a 30-m spatial resolution EVI product every 16 days; however, this is often prolonged by cloud cover (Loveland & Dwyer, 2012; Wulder, Masek, Cohen, Loveland, & Woodcock, 2005) which has hampered vegetation studies. Studies have employed data-mining techniques and the use of multiyear Landsat data to model regional vegetation and facilitate a finer temporal scale of observation (Fisher et al., 2006; Melaas et al., 2013; Nijland et al., 2016). Nijland et al. (2016) acquired Landsat data from 1984 to 2014 and used a double sigmoid function to interpolate regional annual vegetation cycles within western Alberta, Canada. Melaas et al. (2016) adapted these methodologies to incorporate a cubic spline function to interpolate annual transition dates and better portray seasonal vegetation cycles within heterogeneous forests. While these methods are able to accurately calculate important average annual transition dates at a regional scale, it is difficult to accurately depict annual changes as results are attributed to average change across a broad range of years rather than a single target year (Baumann, Ozdogan, Richardson, & Radeloff, 2017).

1.3 | Data fusion for vegetation monitoring

In order to model inter-annual change at moderate spatial scales more accurately, one alternative is to fuse Landsat and MODIS data sets. Dynamic Time Warping (DTW) is a fusion technique that was first developed as a speech recognition algorithm (Sakoe & Chiba, 1978) and has been proven capable of determining patterns in corresponding remote-sensing data sets (Baumann et al., 2017; Berman et al., 2018; Petitjean, Inglada, & Gançarski, 2012). It has the ability to increase temporal density of historic time series by shifting annual dates based on rule sets generated from complimentary datasets. Baumann et al. (2017) used DTW methods to fuse MODIS and Landsat EVI data sets to examine vegetation cycles at individual sites from 2000 to 2012 in Eastern USA. They determined that, compared to ground camera data, the DTW Landsat product was more accurate than MODIS alone at predicting transition dates. Berman et al. (2018)

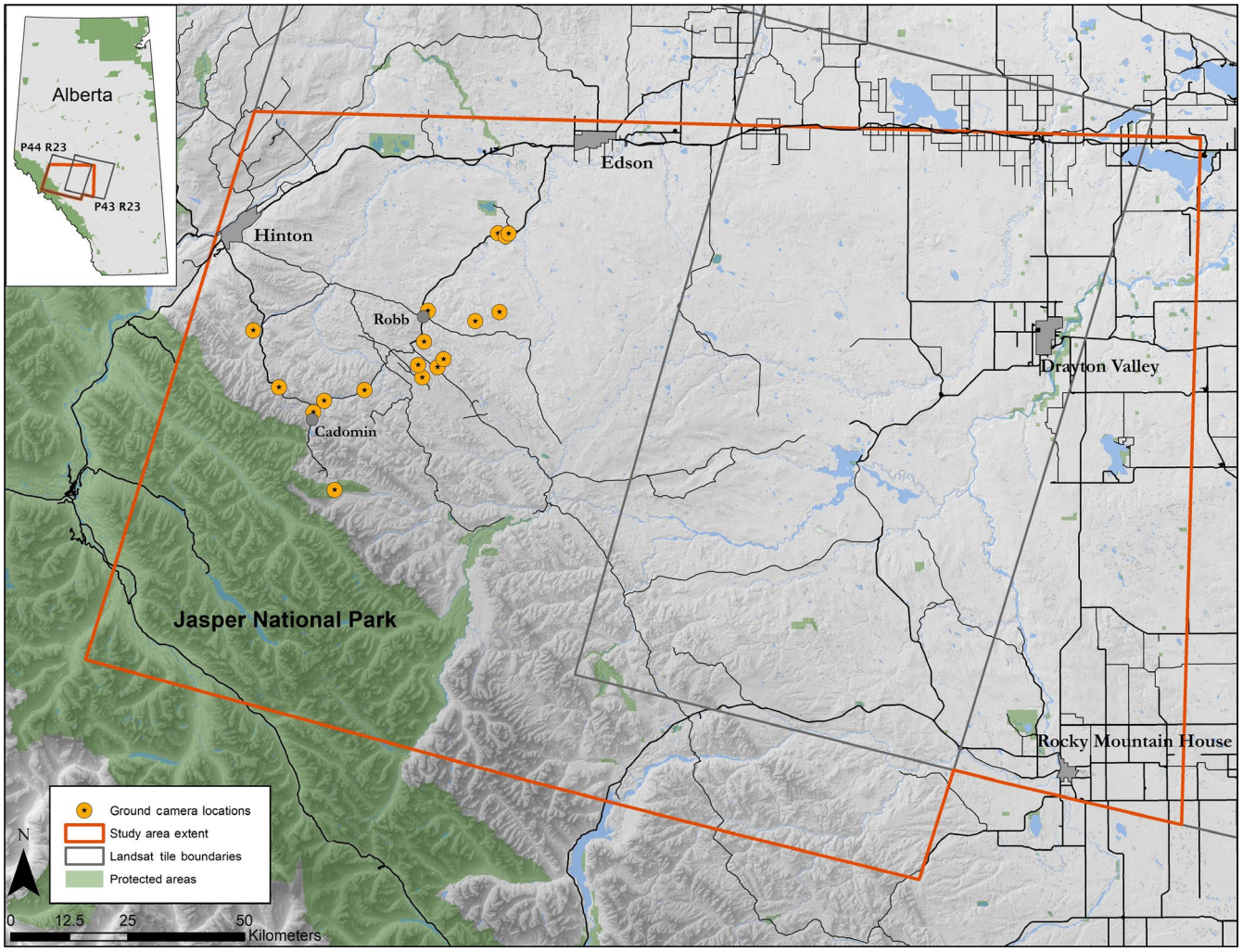

FIGURE 1 Study area located in Western Alberta, Canada, showing study area extent and ground camera locations [Colour figure can be viewed at wileyonlinelibrary.com]

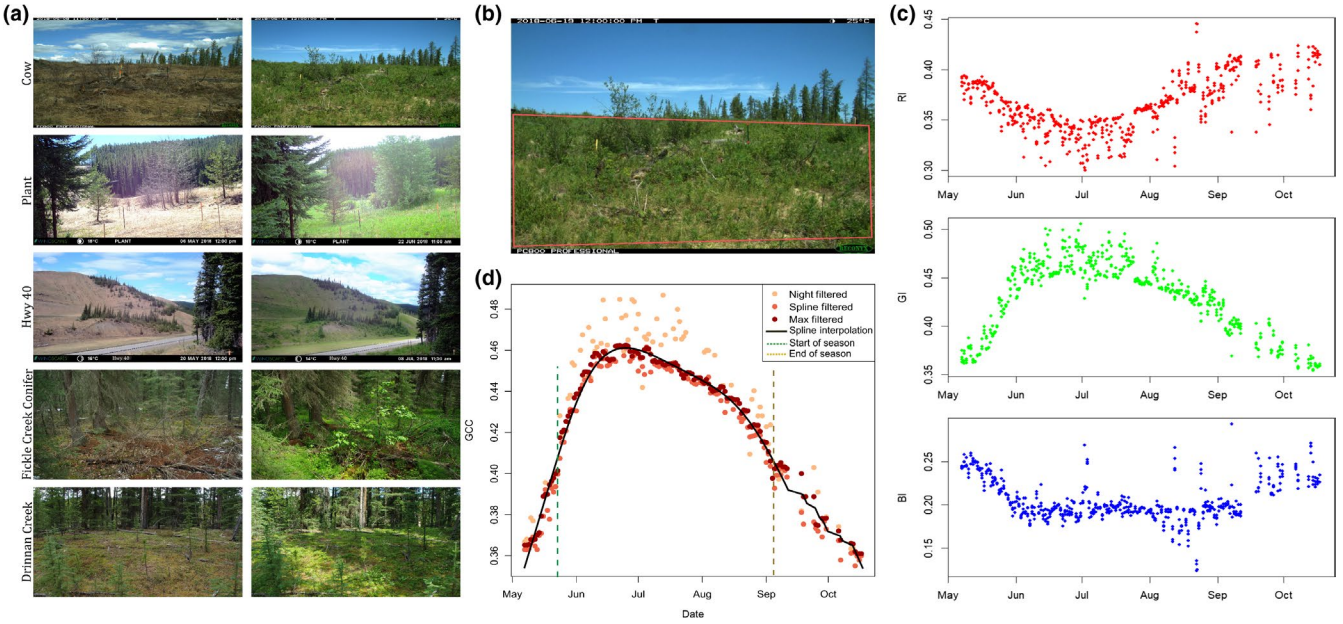

FIGURE 2 Ground camera extraction process: (a) an example of imagery before (left) and after (right) start of season (SOS) from five example sites within this study; (b) an example of a region of interest from which values will be extracted; (c) an example of the red/green/blue index values extracted by the Phenopix package which will be used to calculate GCC (Green Chromatic Coordinates); and (d) the output of the filtering process with max filter (dark red being values) ultimately used with a cubic spline fit to the data and SOS and end of season (EOS) dates extracted [Colour figure can be viewed at wileyonlinelibrary.com]

adapted these techniques to accurately assess inter-annual change in regional snow cover at a fine spatial scale with greater than 80% accuracy when compared to ground cameras. Results were further used to model grizzly bear response to varying snow conditions (Berman, Coops, Kearney, & Stenhouse, 2019). These proof-of-concept studies highlight the opportunity to use dynamic time warping to model vegetation dynamics over a large region at a fine spatial scale.

Here, we examine vegetation trends over a large mountainous and forested region in western Alberta, Canada, by fusing MODIS and Landsat imagery using DTW and spline curve fitting. The new method, which we term Daily Remote Inference of VEgetation (DRIVE), is used to derive a 30-m daily vegetation product from 2000 to 2018. In addition, we use the DRIVE product to determine how vegetation transition dates have varied through time across elevation and land cover classes to determine the overall effect of climate change across the landscape. While we expect there will be a general trend towards earlier green-up dates, we hypothesize that the degree of this change will vary by elevation and land cover classes with larger variations occurring at lower elevations and within open habitat such as shrub and herbaceous areas as these will be more accurately analyzed via satellite. Ultimately, we provide a product to enable the analysis of how vegetation cycles are changing seasonally and annually under a changing climate and the effects on different plant and wildlife communities.

2 | STUDY AREA

We conducted this analysis within the Yellowhead Bear Management Area, over a 31,180-km^2 area in west central Alberta (Figure 1). Jasper National Park defines the westernmost extent of the study area and is a protected mountainous region. To the east, the landscape shifts from mountainous to rolling foothills. In the foothills, there are historic and ongoing anthropogenic disturbances in the form of recreation, oil and gas extraction, coal mining and forestry operations. There are four natural subregions in the Yellowhead area: alpine, subalpine and upper/lower foothills (Achuff, 1994). The most common tree species in the area is *Pinus contorta* (lodgepole pine). Other common tree species include *Picea mariana* (black spruce), *Picea glauca* (white spruce), *Populus tremuloides* (trembling aspen), *Populus balsamifera* (balsam poplar) and *Abies balsamea* (balsam fir). Understorey species in this area include graminoids and forbs such as *Trifolium* spp., *Heracleum lanatum*, *Taraxacum officinale* and *Equisetum* species. Berry species such as *Vaccinium myrtilloides*, *Vaccinium membranaceum* and *Shepherdia canadensis* are plentiful throughout the study area and become available during late summer into early fall (Munro, Nielsen, Price, Stenhouse, & Boyce, 2006).

3 | METHODS

3.1 | Data

3.1.1 | MODIS data

A total of 1,624 500-m spatial resolution MODIS V6 MOD13A1 and MYD13A1 images were downloaded from both the Aqua and Terra platforms from January 1st, 2000 to December 30th, 2018 for tiles H10V03 and H11V03. MOD13A1 and MYD13A1 EVI products

consist of 16-day composites of the highest quality vegetation index data for that period (Huete et al., 2002). When coupled, these datasets produce a composite every eight days. MODIS EVI data and corresponding pixel assurance data from both Aqua and Terra sensors were extracted and stacked separately in eight -day intervals annually from days 1 to 365. Pixels were masked to extract only the highest quality, clear-sky data, based on quality assurance datasets (Didan, Barreto Munoz, Solano, & Huete, 2015).

3.1.2 | Landsat data

Preprocessed 30-m resolution Landsat EVI data products for Landsat Thematic Mapper (TM), Enhanced Thematic Mapper Plus (ETM+), and Operational Land Imager (OLI) sensors and corresponding pixel quality assurance were acquired from the USGS archive (https://earthexplorer.usgs.gov/) for January 1st, 2000 to December 31st, 2018. Two WRS-2 tiles (path/rows: 43/23, 43/24) cover the study area and 1,186 images were subsequently downloaded from the USGS website for both tiles. Images were masked using corresponding pixel quality assurance values. For TM, ETM + and OLI sensors, only pixels with corresponding clear pixel quality assurance (1, 66, 130 for TM and ETM + and 1, 322, 386, 834, 898, 1,346 for OLI) were used. This eliminated pixels containing cloud, cloud shadow, snow/ice and water from the analysis following methods of Melaas et al., 2013; Melaas et al., 2016 and Nijland et al., 2016.

While EVI data range from 0 to 1, both Landsat and MODIS multiply raw EVI values by 10,000 to transform to integer data. These values were not altered in this analysis.

3.1.3 | Camera data

Digital time-lapse cameras were used to acquire daily vegetation ground data throughout the growing seasons of 2009, 2010 and 2018. Cameras were installed at 17 locations along an elevation gradient and set up with a wide field of view (FOV) to capture the surrounding areas and trends in canopy and understorey vegetation for

TABLE 1 Ground camera site details located in UTM zone 11and Landsat tile P44R23

Site	Year	Easting	Northing	Elevation	Camera type	MODIS tile	Site type
Hwy 40	2018	5,882,405	470,929	1,620	Wingscapes TimelapseCam Pro	H10V03	Non-Forested
Pond	2018	5,882,302	489,235	1,371	Wingscapes TimelapseCam Pro	H10V03	Non-Forested
Huck	2018	5,885,343	501,512	1,366	Wingscapes TimelapseCam Pro	H10V03	Non-Forested
Hi	2018	5,887,658	504,729	1,318	Wingscapes TimelapseCam Pro	H10V03	Non-Forested
Swamp	2018	5,889,402	505,988	1,257	Wingscapes TimelapseCam Pro	H10V03	Non-Forested
Cow	2018	5,892,997	501,705	1,252	Reconyx PC800	H10V03	Non-Forested
B2m	2018	5,887,995	500,568	1,247	Wingscapes TimelapseCam Pro	H10V03	Non-Forested
Rig	2018	5,899,801	517,637	1,161	Wingscapes TimelapseCam Pro	H11V03	Non-Forested
Plant	2018	5,897,700	512,533	1,121	Wingscapes TimelapseCam Pro	H11V03	Non-Forested
Low	2018	5,916,659	516,847	998	Wingscapes TimelapseCam Pro	H11V03	Non-Forested
Cardinal Divide	2010	5,860,769	483,439	2,025	Pentax K100D	H10V03	Non-Forested
Drinnan Creek	2010	5,894,401	465,076	1,356	Pentax K100D	H10V03	Forested
Cadomin Mixed	2009	5,877,276	478,427	1,484	Pentax K100D	H10V03	Forested
Cadomin Conifer	2009	5,879,755	480,660	1,458	Pentax K100D	H10V03	Forested
Bryan Spur Mixed	2009	5,899,684	502,319	1,093	Pentax K100D	H11V03	Forested
Fickle Lake Mixed	2009	5,916,668	519,136	970	Pentax K100D	H11V03	Forested
Fickle Lake Conifer	2009	5,916,058	518,537	951	Pentax K100D	H11V03	Forested

Sites were distributed along elevation gradients capturing a variety of key understorey food species within the study area.

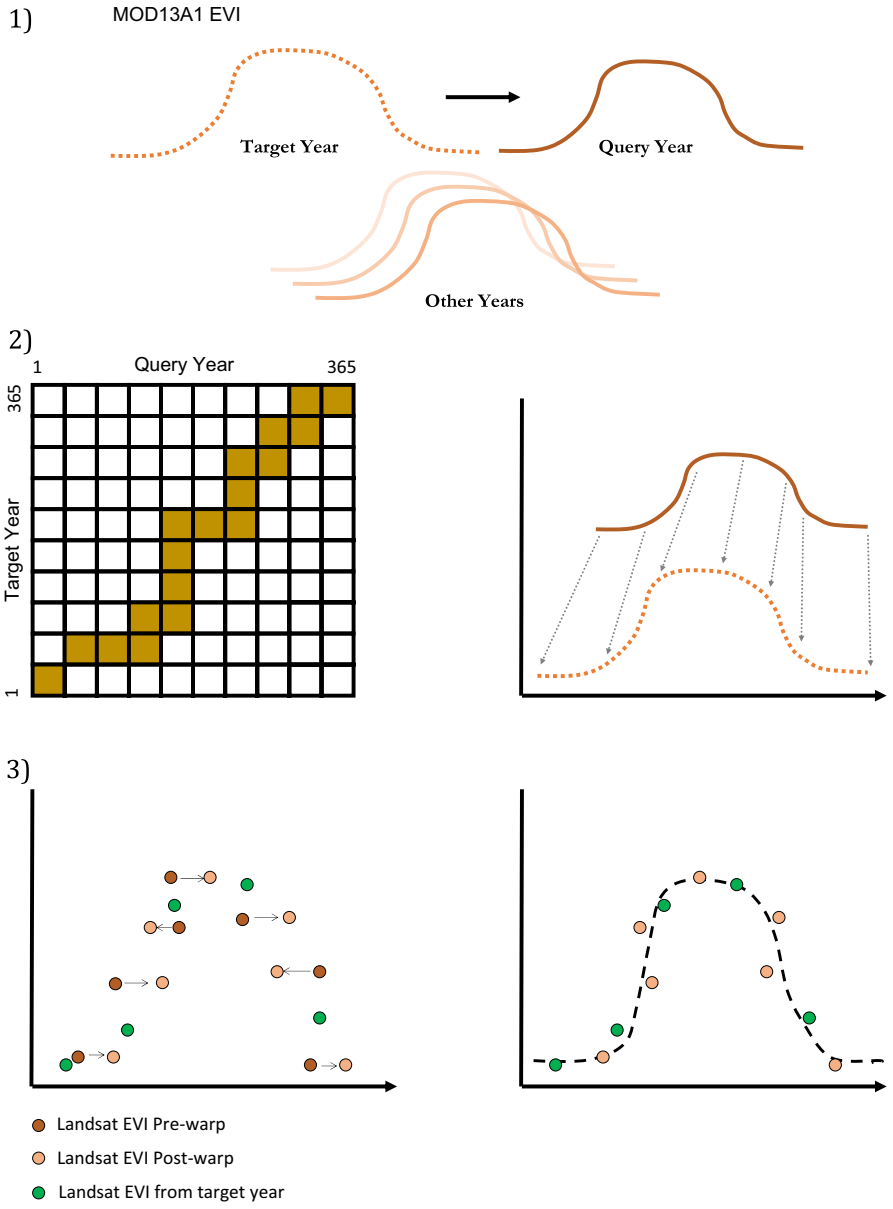

FIGURE 3 Dynamic time warping steps. (1) Define target and query years. (2) Apply the Dynamic Time Warping algorithm and create the rule set to inform the warp. (3) Rearrange Landsat Enhanced Vegetation Index (EVI) based on the generated rule set and fit a spline to interpolate curve with rearranged values [Colour figure can be viewed at wileyonlinelibrary.com]

each site (Figure 2a) (Vartanian et al., 2014). Sites selected in 2018 were generally open (non-forested) to allow better detection of variations in understorey vegetation, while sites in 2009 were selected with canopy cover (forested). In 2010, sites were a mix of locations with and without canopy cover. Understorey plant communities across these sites were therefore a mixture of grasses, forbs and shrubs and were of varying species compositions. Camera models varied depending on the year data were collected; however spatial resolution of the camera images was similar (Table 1). Cameras were mounted on trees, between 2 and 3 m above ground level with varying directions of observation for each site and with an average spatial extent between 30 and 60 m. Between three and five time-lapse images were captured daily between 11:00 hours and 13:00 hours at half-hour to hourly intervals (Figure 2a.) and images were stored on memory cards.

Start and end of season dates were derived using the Phenopix package (Filippa et al., 2016) in R statistical software (R Core Team, 2018). Regions of interest (ROIs) were drawn to capture vegetation over the entire FOV (Figure 2b). Red/green/blue (RGB) index values were extracted as an average over the entire ROI for each site (Figure 2c). Green Chromatic Coordinates (GCC) were calculated using Equation 1 and values were filtered at three levels to remove outliers. The first filter was the night filter, which used brightness values to

$$GCC = \frac{GI}{RI + BI + GI} \quad (1)$$

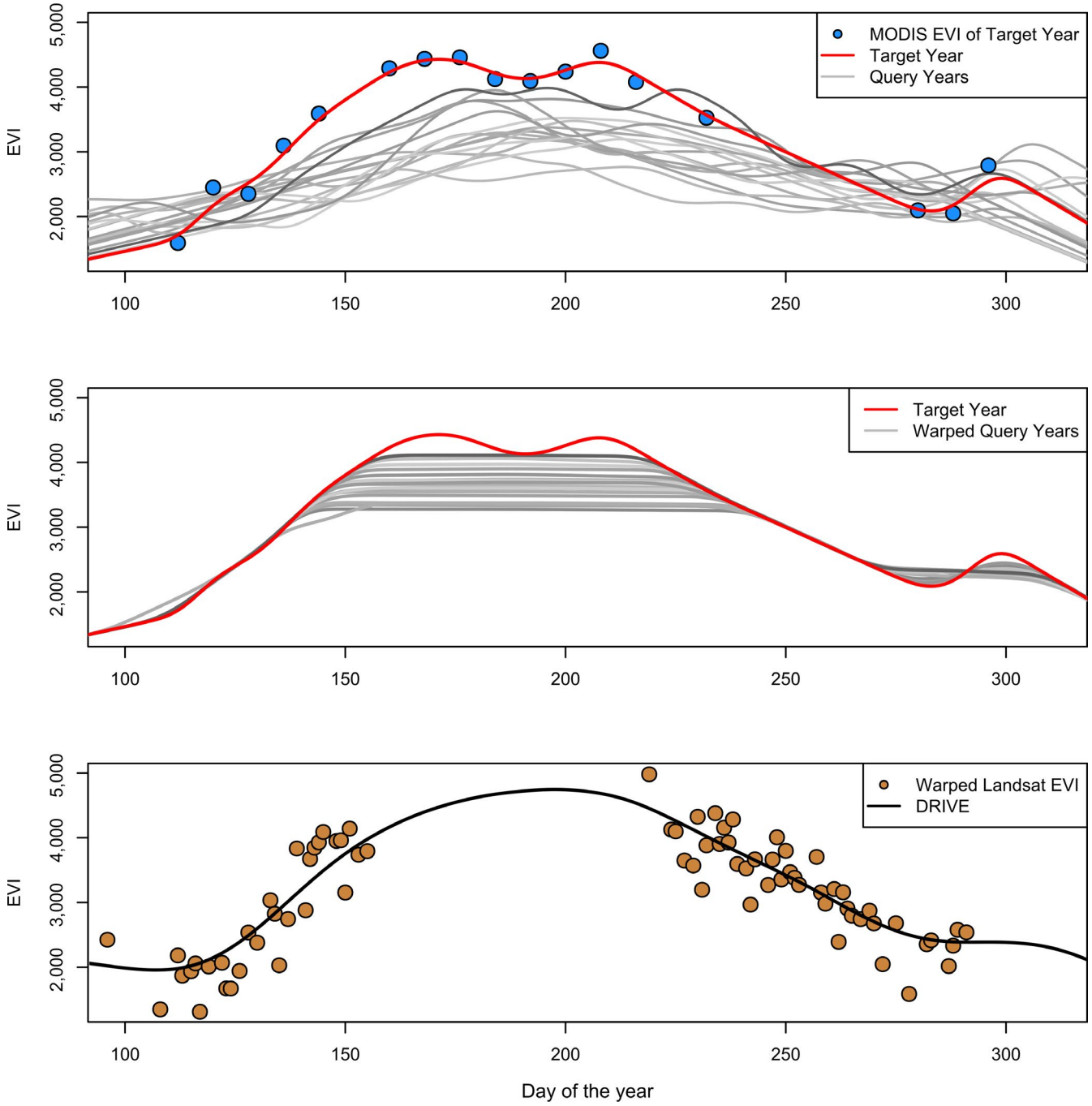

FIGURE 4 Example of warped results from Cow camera site. (TOP) MODIS Enhanced Vegetation Index (EVI) from target year (2018) is interpolated. In greyscale are all corresponding query years. (MIDDLE) Example of all query years post application of the warping algorithm being warped to said target year. (BOTTOM) Results of rule set generated from warping algorithm being applied to Landsat EVI and then interpolated using a cubic spline [Colour figure can be viewed at wileyonlinelibrary.com]

The first filter was the night filter, which used brightness values to eliminate points occurring under conditions of low light caused by clouds and shadows. The second was the spline filter, which is based on recursive spline smoothing and residual computation, thereby removing all values that did not lie within a certain residual envelope (Migliavacca et al., 2011). Thresholds used were two standard deviations below and 1.5 standard deviations above mean GCC values. The third filter used was the max filter which identifies 90th percentile residual values in a three-day moving window (Sonnentag et al., 2012) (Figure 2d). Cubic splines were fit for each time series of images (Figure 2d.).

3.1.4 | Land cover and digital elevation model data

We analyzed how vegetation cycles changed under differing land cover types and across elevation gradients from 2000 to 2018. Land

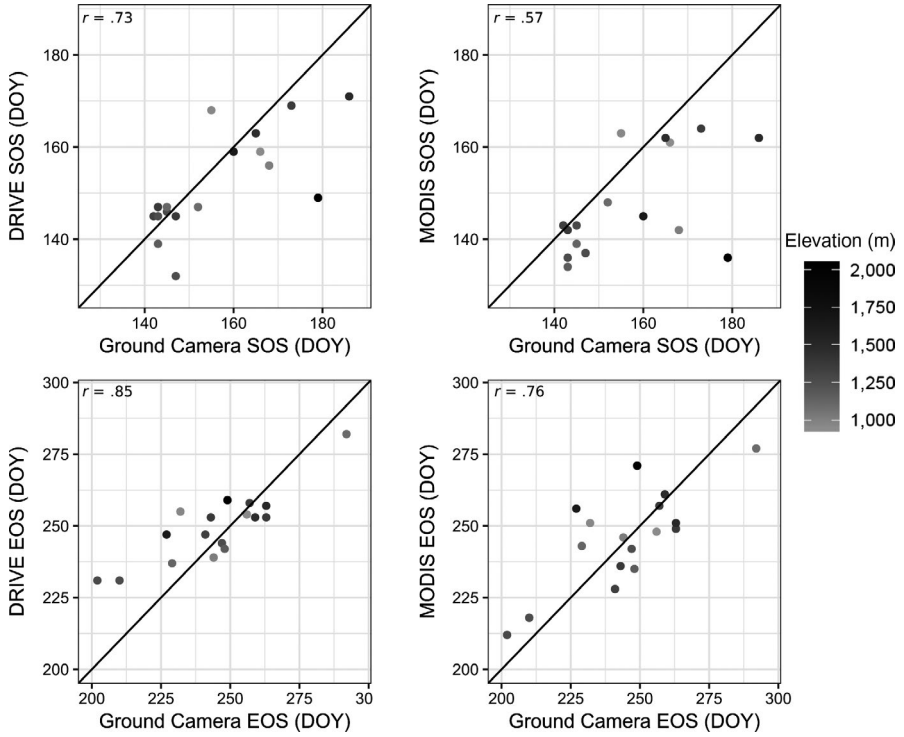

FIGURE 5 Comparison of results between DRIVE (Daily Remote Inference of VEgetation) as compared to ground camera start of season (SOS) and end of season (EOS) and MODIS (Moderate Resolution Image Spectroradiometer) as compared to ground camera SOS and EOS and EOS. DOY, day of year

cover classes were derived from Hermosilla, Wulder, White, Coops, and Hobart (2015), who produced a 30-m spatial resolution Landsat-derived land cover map of the region in 2016, which included six classes: bryoids, broadleaf, coniferous, herbs, mixed wood and shrubland. A 30-m digital elevation model (DEM) was obtained from the Shuttle Radar Topography Mission (SRTM; Farr et al., 2007) which we reclassified into elevation classes in increments of 200 m from 500 to 2,100 m a.s.l.

3.2 | Dynamic time warping

Dynamic Time Warping (see Figure 3) involves first creating a rule set from MODIS data and then fitting curves to a time series of values — in this case EVI — as follows (also see Baumann et al., 2017; Berman et al., 2018).

First, annual vegetation curves were created per pixel using the stacked preprocessed MODIS EVI data, where the band order corresponded to day of year (DOY) from 1 to 365. MODIS EVI data values were spatially smoothed using a 3 × 3 low-pass filter to eliminate spatial noise. Results were calculated with 50% weighting on the centre pixel and 50% on the neighbourhood (Berman et al., 2018). Annual vegetation curves were then obtained through cubic spline interpolation (Melaas et al., 2016) and these were further smoothed using a Gaussian filter with a sigma value of 4. Linear interpolation was implemented if a temporal gap between values exceeded eight days, to avoid extreme values (Berman et al., 2018).

Second, rule sets between query years and target years were generated. To accomplish this, we first defined an annual curve as the target year. All other years consequently became known as the query years. All query years were individually warped to each target year using a 365 × 365 matrix with each cell containing the Euclidean distance between target and query year MODIS EVI values (Baumann et al., 2017; Berman et al., 2018). Theoretically, the warp path possibilities are exponentially high; however, a rule set was generated based on the path which minimized the Euclidean distance between target and query MODIS EVI, with curves starting at day of the year 1 and ending at day 365. The algorithm used a 50-day window in which to restrict the resultant rule sets such that if observations were >50 days apart, a rule set was not able to form a relation (Berman et al., 2018). This second step was repeated until all years had become a target year generating a rule set for every year.

In the final step, Landsat EVI observations were rearranged based on generated rule sets. All query year Landsat EVI observations contained within each MODIS pixel were rearranged to fit with target year observations. Target year observations were not rearranged as they signify real values. In situations where multiple values were warped to the same day of year, the mean of all values for that day was used (Berman et al., 2018). Landsat EVI vegetation curves were created for every year by iteratively generating rulesets with that year becoming the target year and having all other years (query years) warped to said target year. Observations for each year were interpolated using similar parameters as in interpolation of MODIS

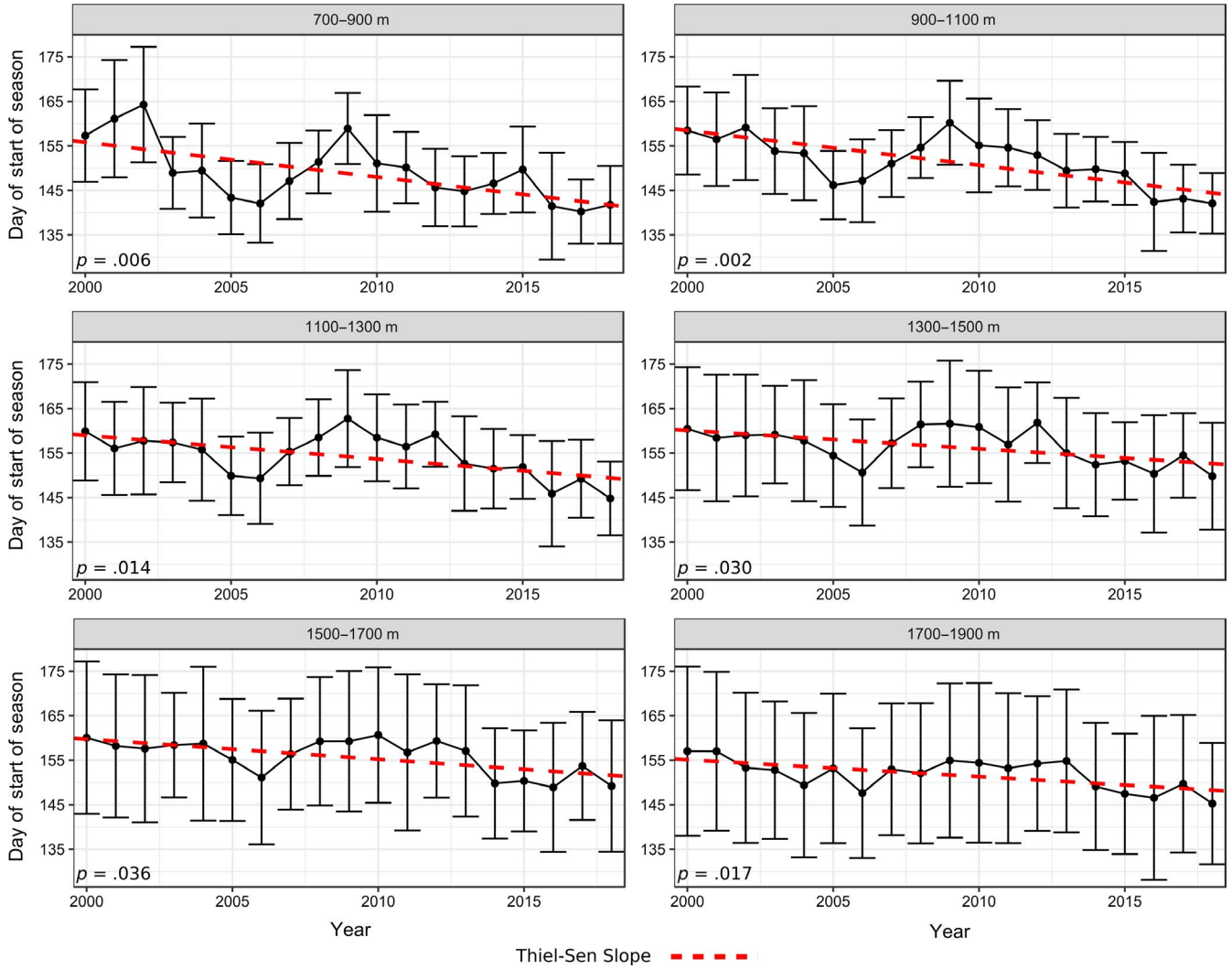

FIGURE 6 Average day of start of season (SOS) per year across 6 elevation classes with error bars representing one standard deviation form the mean [Colour figure can be viewed at wileyonlinelibrary.com]

EVI, the key difference being, however, that the sigma value in the Gaussian filter used for Landsat EVI was increased to 13 (determined by parameter tuning). This increased smoothing on all spline curves reducing noise and aided in comparing Landsat EVI to ground camera data (see Figure 4 for an example). This technique and the resultant product is here called DRIVE (Daily Remote Inference of VEgetation).

3.3 | Validating DRIVE

3.3.1 | Seasonal metrics

To compare DRIVE to ground camera data, determine accuracy of DRIVE in relation to MODIS data, and assess how vegetation cycles varied inter-annually, seasonal metrics were extracted from the ground cameras, DRIVE, and MODIS curves. Seasonal metrics were used to bridge the gap between GCC and EVI values as while their numerical values are not comparable, their trends are (see Melaas et al., 2016 for example). Previous methods utilize inflection points to define start of season (SOS) and end of season (EOS; Beck et al., 2006); however the inability to define inflection points within a cubic spline make this method not feasible. In this study, SOS and EOS were calculated by splitting vegetation curves into two sections at the seasonal maximum. Minimum values were then calculated before and after the seasonal maximum to define the lower extent of the range of values before and after seasonal maximum. The DOY (day of year) value corresponding to the half-maximum (50% of seasonal maximum) values prior to seasonal maximum is designated as the SOS date and the DOY value corresponding to the half-maximum post seasonal maximum is designated as the EOS date.

3.3.2 | Accuracy

In order to ensure accuracy of DRIVE, SOS and EOS dates were compared to those derived from the 17 ground camera sites. We also compared the ground camera data to the original MODIS

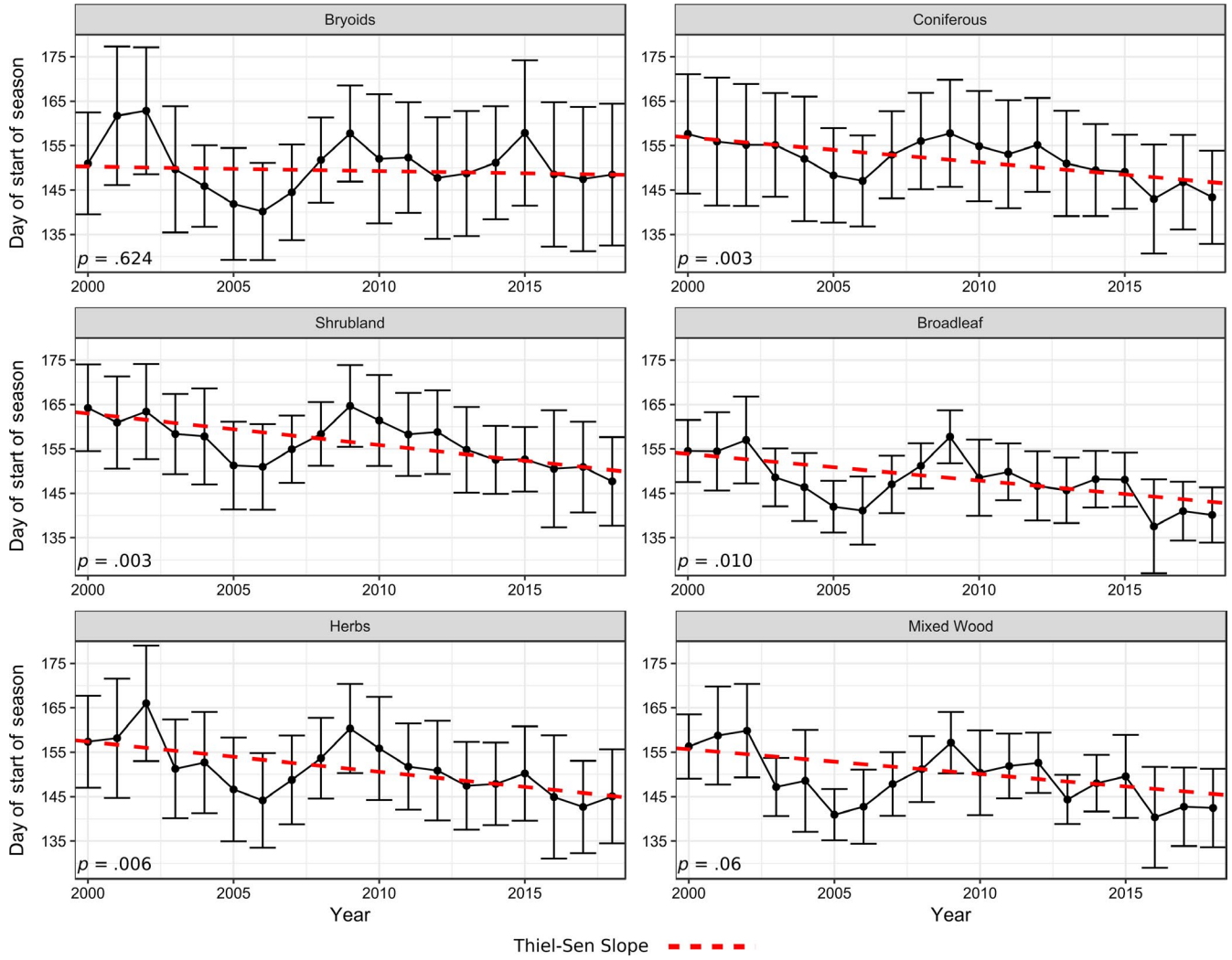

FIGURE 7 Average day of start of season (SOS) per year across six land cover classes with error bars representing one standard deviation from the mean [Colour figure can be viewed at wileyonlinelibrary.com]

product used within the warp to quantify improvements in accuracy due to increased spatial resolution (from 500 m to 30 m). Correlation coefficients (*r*) and Root Mean Squared Error (RMSE) were used to assess accuracy, while root mean bias was used to determine whether DRIVE and MODIS were over- or under-predicting SOS and EOS. Mean absolute error (MAE) was used to calculate the difference in days between ground cameras and DRIVE/MODIS results.

3.4 | Change in vegetation cycles from 2000 to 2018

3.4.1 | Start of season and end of season layers

Dates of the start and end of the growing season were calculated from day 105 to 310 for each year to isolate green-up and senescence signals based on visual assessment and methods proposed by Nijland et al. (2016). For each time series of observations within this period a curve was extracted along with the half-maximum and half-minimum using the same process used to extract seasonal metrics. Results were masked for (a) having an EVI amplitude of less than 1,000 (equivalent to the amplitude of 0.1 used in Nijland et al. 2016) as they were deemed to have little to no green-up and (b) having non-feasible SOS values considered to be outside the main growing season (i.e. having a SOS less than day 125 or a SOS later than day 200) (Nijland et al., 2016).

We used random stratified sampling to extract vegetation SOS and EOS dates across elevation classes and land cover classes from 2000 to 2018. For each elevation and land cover class, 500 random points were generated and used to extract values from SOS and EOS layers. Random points were generated annually in the case of land cover classes to account for yearly changes. The mean of extracted values was calculated at every elevation and land cover class. To assess the statistical significance of the observed trend over a time, we used a Mann–Kendall trend test (de Beurs &

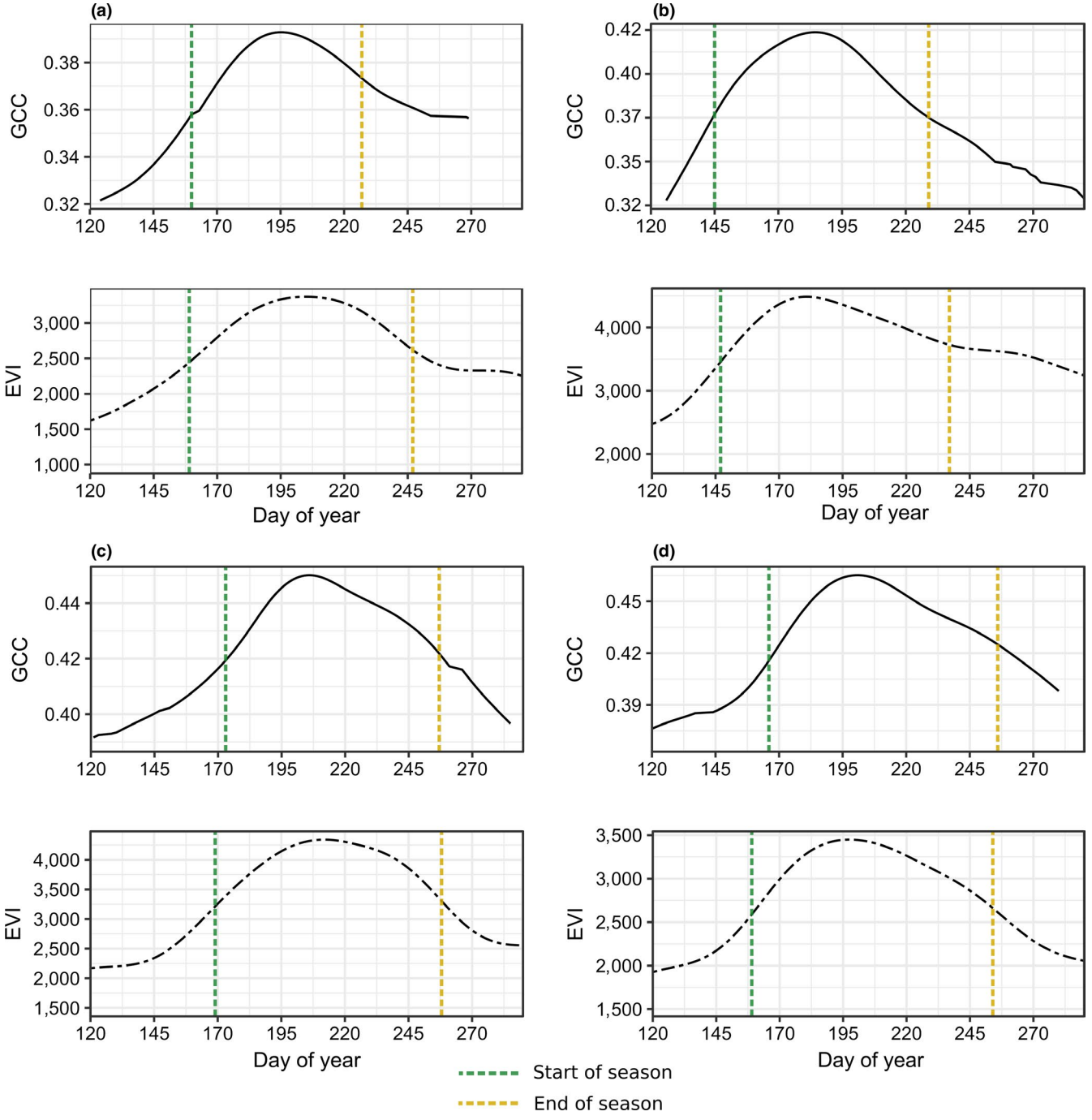

FIGURE 8 Comparison of ground camera vegetation curves Green Chromatic Coordinates (GCC) to DRIVE (Daily Remote Inference of VEgetation) vegetation curves Enhanced Vegetation Index (EVI) at four sites. (a) Hwy 40, (b) Plant, (c) Drinnan Creek, (d) Fickle Lake Conifer [Colour figure can be viewed at wileyonlinelibrary.com]

Henebry, 2005). Slopes of trends were estimated using the Theil–Sen slope estimator.

4 | RESULTS

Using the daily coverage of DRIVE instead of the 16-day cover of Landsat increased the number of cloud-free, snow-free and good quality observations at our study sites from an average of 7.2 to 137.3 observations per year. This marked increase in average annual usable observations allowed for the creation of a temporally dense time series capable of interpolating EVI values over the season.

4.1 | Validation results

For the 17 ground camera sites distributed over three years (Table 1) DRIVE SOS and EOS resulted in higher correlations (SOS: $r = 0.73$, RMSE = 10.3; EOS: $r = 0.85$ and RMSE = 13.0) than MODIS

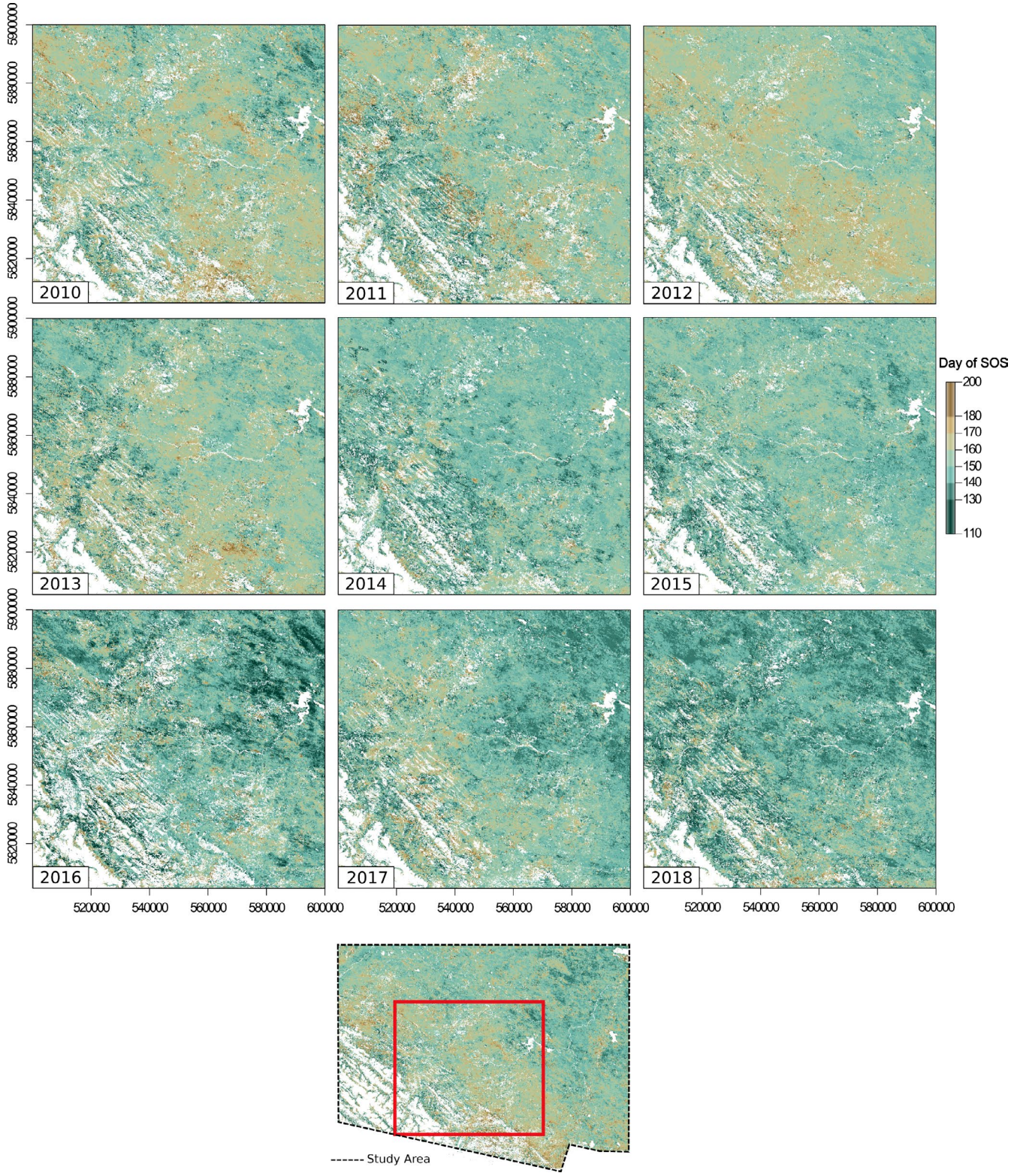

FIGURE 9 Start of season (SOS) layers per year from 2010 (top left corner) proceeding across and down ending with 2018 (bottom right corner). Bottom panel represents the extent of view within the study area. Note: absent pixels are where warp did not perform well or accurately [Colour figure can be viewed at wileyonlinelibrary.com]

data alone (SOS: r = 0.57, coefficient RMSE = 15.1; EOS: r = 0.76, RMSE = 13.5) (Figure 5). Both DRIVE and MODIS underestimated the timing of SOS with a mean bias of −4.2 days for DRIVE and −9.7 days for MODIS. The MAE of SOS compared to ground camera data was 7.17 days using DRIVE and 10.35 days using MODIS. With EOS we found an over estimation in the DRIVE vegetation

product with a mean bias of 4.2, while there was less of an overestimation for MODIS with a mean bias of 1.1. The MAE between EOS calculated using DRIVE when compared to ground camera data and MODIS when compared to ground camera data was 10.76 and 11.35 days respectively.

4.2 | Long-trend vegetation cycle changes across land cover and elevation

We observed a significantly decreasing trend over the study period in average SOS for all elevation classes ($p < 0.05$) and for all land cover classes except for bryoids ($p = 0.624$) and mixed wood ($p = 0.058$). Using the Thiel–Sen slope estimator, the deepest trend slope occurred in elevation classes 700–900 m and 900–1,100 m with SOS beginning 0.78 days earlier per year. For land cover classes, the most drastic change occurred within the shrubland class with SOS beginning 0.71 days earlier per year (Figures 6, 7).

5 | DISCUSSION

5.1 | Dynamic time warping

Our results show that the DRIVE approach overcomes the inherent trade-off between coarse spatial resolution of MODIS data and the coarse temporal resolution of Landsat data. With Dynamic Time Warping (DTW) and DRIVE, we used MOD13A1 EVI data to characterize annual regional vegetation and form a basis for rearranging multiyear Landsat EVI imagery to create a 30-m, daily vegetation product. Our methods make it possible to quantify seasonal and annual variability in vegetation across very large regions, historically for the past two decades. In the Yellowhead region of Canada, we found DRIVE was able to increase the spatial resolution of MODIS data (at 500 m) when using high-resolution ground cameras as validation, thus increasing accuracy in determining SOS and EOS dates at finer spatial scales than when using MODIS data alone. We were able to predict SOS within seven days and EOS within 10 days with ground cameras with similar results being reported in Baumann et al. (2017) and Nijland et al. (2016). The better results for SOS compared to EOS may be related to the SOS signal being stronger than the EOS signal (Nijland et al., 2016) and may also relate to lower solar elevation and sun angle at EOS and there being a stronger signal from conifer species as sun cannot penetrate to the understorey (Kobayashi et al., 2016). The correlation between DRIVE and ground camera data across 17 forested and non-forested sites with varying species composition displays its ability to capture spatial patterns in vegetation across our study area beyond simple elevation trends. Moreover, our results indicate that DRIVE is influenced by both over- and understorey vegetation, dependent on land cover type. The fact that DRIVE detected SOS and EOS within open- and moderate-canopy conifer forests in our study area suggests the method is able to detect understorey changes. In broadleaf forests, we suspect that the vegetation signals are more strongly influenced by overstory vegetation.

Previous work has shown the usefulness of DTW in quantifying annual vegetation cycles; however, it was only done at point locations or over small areas and never over such a large time period (Baumann et al., 2017). Our study expands on this work and demonstrates the utility of DTW and DRIVE in quantifying vegetation dynamics across a large region and over 18 years. We further demonstrated the ability of DTW to describe floristically heterogeneous plant communities, whereas previous work with DTW in vegetation has been focused more narrowly on alpine environments and deciduous forests (Baumann et al., 2017; Huseby et al., 2005). We attribute this advance to the use of cubic splines within the interpolation process, which provide a more natural fit and as a result better characterize differences between vegetation types (see Figure 8 for example) than in previous studies that characterized and constrained vegetation patterns using double sigmoid or double logistic functions (Baumann et al., 2017; Fisher et al., 2006; Melaas et al., 2013; Nijland et al., 2016). Cubic spline interpolation aided in smoothing data and eliminating noise while still preserving differences in vegetation trends between pixels and within individual communities. The use of cubic splines also helped in preserving SOS and EOS dates after pixels showing snow and ice cover were removed. We have confidence in the accuracy of using a spline fit based on the correspondence between the DRIVE-based vegetation curves for individual sites and those obtained from the ground camera data.

Baumann et al. (2017) highlighted a potential limitation of DTW in that accuracy was unknown within different land cover classes. We validated DRIVE across several different land cover classes (e.g. shrubland, mixed and conifer forest, cut-blocks) and showed that accuracies were similar across all land cover classes. However, visual inspection suggests DRIVE performed poorly at higher elevation sites, along forested sides of mountains and hills, in places with dense conifer canopy cover and in places with evergreen vegetation or understories, as indicated by pixels being excluded when creating SOS and EOS layers (Figure 9). These discrepancies are similar to ones experienced by Nijland et al. (2016). In cases where there is dense conifer or evergreen vegetation, little to no leaf-out is detected and a substantial EVI signal is observed as soon as these areas are snow-free. What little leaf-out that does occur is then negligible when combined with this initial signal, and thus an earlier than feasible SOS date is detected. Similar processes may be at work along hill and mountainsides where vegetation is not being detected due to angle of observation and the inability of the sensor to observe understorey vegetation through the canopy.

We compared DRIVE output to existing MODIS data outputs, as the MODIS satellite imagery is a globally recognized vegetation product and one that is used in many global comparisons. MODIS EVI is the best available vegetation product, therefore we believe comparing field based data to MODIS EVI is reasonable despite heterogeneity of our fine-scale sites. While we acknowledge that it is

not possible to independently compare due to the use of MODIS EVI data in building the rule sets within the DTW algorithm, one possible approach would be to resample DRIVE output up to 500 m and observe whether the resampled DRIVE data are comparable to the initial MODIS data. Although not the focus of this study, additional tests such as this could be applied to give further confidence to the approach.

5.2 | Inter-annual vegetation trends

Within this study, we quantified annual change in SOS dates throughout the past two decades and demonstrated that, overall, SOS is shifting earlier across all elevation and land cover classes except for bryoids and mixed wood forest. These results were significant and indicate a measurable effect of changing climate within our study area. At higher elevations and within conifer forests, trends were smaller with larger error than when compared to lower elevations and other land cover classes corresponding to warp inaccuracies in these classes. Similar climate-driven shifts in spring vegetation cycles have been reported in many studies throughout North America and the world (Chuine & Beaubien, 2001; Chmielewski & Rötzer, 2002; Schwartz, Ahas, & Aasa, 2006; Beaubien & Hamann, 2011). By contrast, vegetation shifts at the end of the growing season were less apparent, likely due to a weaker and less abrupt end of season spectral signal.

A shift toward earlier spring green-up has important implications for plant communities, carbon sequestration, and wildlife whose foraging patterns follow seasonal vegetative food patterns. For example, earlier availability of vegetation may create a temporal mismatch between what food is available compared to what food is required in animal diets for that time of the year. There is evidence such mismatch is already occurring for some species, such as for grizzly bears foraging on *Shepherdia canadensis* (Laskin et al., 2019). Our results further show that similar spring advancement may be happening for other more important food species for grizzly bears and other wildlife species in the region. However, due to poor EOS signal, it is unclear whether the growing season is shifting towards earlier dates or the length of the growing season is increasing. Future research is needed on the response of individual vegetative species to climate change in order to better understand the implications for wildlife diets as well as how carbon sequestration is varying within plant communities.

5.3 | Conclusion

With the DRIVE algorithm and product, we were able to portray spatial and temporal vegetation patterns at a 30-m daily scale over a large region and improve upon annual detection of vegetation trends within a heterogeneous environment. We further demonstrated the usefulness of DRIVE through the creation of SOS and EOS metrics capable of quantifying two decades of changing vegetation cycles within varying elevation and land cover classes. We envision several key applications for DRIVE. Primarily DRIVE may be crucial in determining how carbon sequestration is varying amongst different plant communities. Next is in combining the vegetation dynamics with wildlife movement data in order to determine how changing vegetation is affecting wildlife species. Potential changes in animal food supply could result in new patterns of wildlife habitat use and migration. With a 30-m resolution, DRIVE could be used in determining how different industrial land management practices are affecting vegetation cycles locally and determine management strategies to protect key wildlife habitat. Such application of DRIVE to management practices could also be extended to recreational use (e.g. backcountry hiking, off-road vehicle use) in order to minimize the public's impact on wildlife resources at sensitive times. As our ability to characterize fine-scale vegetation cycles in a changing climate improves, so can we improve our land use practices to more effectively manage both the natural and human environment.

ACKNOWLEDGEMENTS

This research was supported by the Grizzly-PAW project (NSERC File: CRDPJ 486175 – 15, Grantee: N.C. Coops, FRM, UBC), in collaboration with fRI Research and FRIAA, Alberta Newsprint Company, Canfor, Cenovus, Repsol, Seven Generations Energy, Shell Canada, TransCanada Pipelines, Teck Resources, West Fraser, Westmoreland Coal, and Weyerhauser. More information can be found at http://paw.forestry.ubc.ca/. We thank staff at fRI research and Bethany Parsons of the University of British Columbia for help in collecting vegetation data.

AUTHOR CONTRIBUTIONS

All authors contributed to the design and implementation of the research, to the analysis of the results and to the writing of the manuscript.

DATA AVAILABILITY STATEMENT

All MODIS and Landsat data is free and open source from the USGS archive (https://earthexplorer.usgs.gov/). All plot level ground data is stored at UBC and may be available upon request.

ORCID

Nicholas C. Coops https://orcid.org/0000-0002-0151-9037
Sean P. Kearney https://orcid.org/0000-0002-5939-1259
Scott E. Nielsen https://orcid.org/0000-0002-9754-0630
A. Cole Burton https://orcid.org/0000-0002-8799-3847

REFERENCES

Achuff, P. L. (1994). *Natural Regions, Subregions and Natural History Themes of Alberta: A classification for protected areas management-updated and revised*. Calgary, AB: Alberta Environment Protection, Parks Services.

Aono, Y., & Kazui, K. (2008). Phenological data series of cherry tree flowering in Kyoto, Japan, and its application to reconstruction of springtime temperatures since the 9th century. *International Journal of Climatology*, *28*(7), 905–914. https://doi.org/10.1002/joc.1594

Bater, C. W., Coops, N. C., Wulder, M. A., Hilker, T., Nielsen, S. E., Mcdermid, G., & Stenhouse, G. B. (2011). Using digital time-lapse cameras to monitor species-specific understorey and overstorey phenology in support of wildlife habitat assessment. *Environmental*

Monitoring and Assessment, *180*(1-4), 1–13. https://doi.org/10.1007/s10661-010-1768-x

Baumann, M., Ozdogan, M., Richardson, A. D., & Radeloff, V. C. (2017). Phenology from Landsat when data is scarce: Using MODIS and dynamic time-warping to combine multi-year Landsat imagery to derive annual phenology curves. *International Journal of Applied Earth Observation and Geoinformation*, *54*, 72–83. https://doi.org/10.1016/j.jag.2016.09.005

Beaubien, E., & Hamann, A. (2011). Spring flowering response to climate change between 1936 and 2006 in Alberta, Canada. *BioScience*, *61*(7), 514–524. https://doi.org/10.1525/bio.2011.61.7.6

Beck, P. S. A., Atzberger, C., Høgda, K. A., Johansen, B., & Skidmore, A. K. (2006). Improved monitoring of vegetation dynamics at very high latitudes: A new method using MODIS NDVI. *Remote Sensing of Environment*, *100*(3), 321–334. https://doi.org/10.1016/J.RSE.2005.10.021

Berman, E. E., Bolton, D. K., Coops, N. C., Mityok, Z. K., Stenhouse, G. B., Moore, R. D., & (Dan)., (2018). Daily estimates of Landsat fractional snow cover driven by MODIS and dynamic time-warping. *Remote Sensing of Environment*, *216*, 635–646. https://doi.org/10.1016/J.RSE.2018.07.029

Berman, E. E., Coops, N. C., Kearney, S. P., & Stenhouse, G. B. (2019). Grizzly bear response to fine spatial and temporal scale spring snow cover in Western Alberta. *PLoS ONE*, *14*(4), e0215243. https://doi.org/10.1371/journal.pone.0215243

Brown, T. B., Hultine, K. R., Steltzer, H., Denny, E. G., Denslow, M. W., Granados, J., … Richardson, A. D. (2016). Using phenocams to monitor our changing Earth: Toward a global phenocam network. *Frontiers in Ecology and the Environment*, *14*(2), 84–93. https://doi.org/10.1002/fee.1222

Chmielewski, F., & Rötzer, T. (2002). Annual and spatial variability of the beginning of growing season in Europe in relation to air temperature changes. *Climate Research*, *19*(3), 257–264. https://doi.org/10.3354/cr019257

Chuine, I., & Beaubien, E. G. (2001). Phenology is a major determinant of tree species range. *Ecology Letters*, *4*(5), 500–510. https://doi.org/10.1046/j.1461-0248.2001.00261.x

Coops, N. C., Hilker, T., Bater, C. W., Wulder, M. A., Nielsen, S. E., Mcdermid, G., … Stenhouse|, G., (2012). Remote Sensing Letters Linking ground-based to satellite-derived phenological metrics in support of habitat assessment Linking ground-based to satellite-derived phenological metrics in support of habitat assessment. *Remote Sensing Letters*, *3*(3), 191–200. https://doi.org/10.1080/01431161.2010.550330

de Beurs, K. M., & Henebry, G. M. (2005). Land surface phenology and temperature variation in the International Geosphere-Biosphere Program high-latitude transects. *Global Change Biology*, *11*(5), 779–790. https://doi.org/10.1111/j.1365-2486.2005.00949.x

Delbart, N., Picard, G., Le Toan, T., Kergoat, L., Quegan, S., Woodward, I., … Fedotova, V. (2008). Spring phenology in boreal Eurasia over a nearly century time scale. *Global Change Biology*, *14*(3), 603–614. https://doi.org/10.1111/j.1365-2486.2007.01505.x

Didan, K., Barreto Munoz, A., Solano, R., & Huete, A. (2015). MODIS Vegetation Index User's Guide (MOD13 Series). Retrieved from http://vip.arizona.edu

Farr, T. G., Rosen, P. A., Caro, E., Crippen, R., Duren, R., Hensley, S., …Alsdorf, D. (2007). The Shuttle Radar Topography Mission. Retrieved from https://www2.jpl.nasa.gov/srtm/SRTM_paper.pdf

Filippa, G., Cremonese, E., Migliavacca, M., Galvagno, M., Forkel, M., Wingate, L., … Richardson, A. D. (2016). Phenopix: A R package for image-based vegetation phenology. *Agricultural and Forest Meteorology*, *220*, 141–150. https://doi.org/10.1016/j.agrformet.2016.01.006

Fisher, J. I., Mustard, J. F., & Vadeboncoeur, M. A. (2006). Green leaf phenology at Landsat resolution: Scaling from the field to the satellite. *Remote Sensing of Environment*, *100*(2), 265–279. https://doi.org/10.1016/J.RSE.2005.10.022

Hermosilla, T., Wulder, M. A., White, J. C., Coops, N. C., & Hobart, G. W. (2015). An integrated Landsat time series protocol for change detection and generation of annual gap-free surface reflectance composites. *Remote Sensing of Environment*, *158*, 220–234. https://doi.org/10.1016/J.RSE.2014.11.005

Huete, A., Didan, K., Miura, T., Rodriguez, E., Gao, X., & Ferreira, L. (2002). Overview of the radiometric and biophysical performance of the MODIS vegetation indices. *Remote Sensing of Environment*, *83*(1–2), 195–213. https://doi.org/10.1016/S0034-4257(02)00096-2

Hufkens, K., Friedl, M., Sonnentag, O., Braswell, B. H., Milliman, T., & Richardson, A. D. (2012). Linking near-surface and satellite remote sensing measurements of deciduous broadleaf forest phenology. *Remote Sensing of Environment*, *117*, 307–321. https://doi.org/10.1016/J.RSE.2011.10.006

Huseby, R. B., Aurdal, L., Eikvil, L., Solberg, R., Vikhamar, D., & Solberg, A.. (2005). Alignment of growth seasons from satellite data. In *International Workshop on the Analysis of Multi-Temporal Remote Sensing Images*, 2005. (pp. 213–216). IEEE. https://doi.org/10.1109/AMTRSI.2005.1469875

Keenan, T. F., Gray, J., Friedl, M. A., Toomey, M., Bohrer, G., Hollinger, D. Y., … Richardson, A. D. (2014). Net carbon uptake has increased through warming-induced changes in temperate forest phenology. *Nature Climate Change*, *4*(7), 598–604. https://doi.org/10.1038/nclimate2253

Kobayashi, H., Yunus, A. P., Nagai, S., Sugiura, K., Kim, Y., Van Dam, B., … Suzuki, R. (2016). Latitudinal gradient of spruce forest understory and tundra phenology in Alaska as observed from satellite and ground-based data. *Remote Sensing of Environment*, *177*, 160–170. https://doi.org/10.1016/J.RSE.2016.02.020

Laskin, D. N. (2017). *Remote sensing of understory plant phenology: A framework for monitoring and projecting the impacts of climate change*. Calgary, AB: University of Calgary.

Laskin, D. N., McDermid, G. J., Nielsen, S. E., Marshall, S. J., Roberts, D. R., & Montaghi, A. (2019). Advances in phenology are conserved across scale in present and future climates. *Nature Climate Change*, *9*(5), 419–425. https://doi.org/10.1038/s41558-019-0454-4

Loveland, T. R., & Dwyer, J. L. (2012). Landsat: Building a strong future. *Remote Sensing of Environment*, *122*(October 2000), 22–29. https://doi.org/10.1016/j.rse.2011.09.022

Ma, S., Pitman, A. J., Lorenz, R., Kala, J., & Srbinovsky, J. (2016). Earlier green-up and spring warming amplification over Europe. *Geophysical Research Letters*, *43*(5), 2011–2018. https://doi.org/10.1002/2016GL068062

Melaas, E. K., Friedl, M. A., & Zhu, Z. (2013). Detecting interannual variation in deciduous broadleaf forest phenology using Landsat TM/ETM+ data. *Remote Sensing of Environment*, *132*, 176–185. https://doi.org/10.1016/j.rse.2013.01.011

Melaas, E. K., Sulla-Menashe, D., Gray, J. M., Black, T. A., Morin, T. H., Richardson, A. D., & Friedl, M. A. (2016). Multisite analysis of land surface phenology in North American temperate and boreal deciduous forests from Landsat. *Remote Sensing of Environment*, *186*, 452–464. https://doi.org/10.1016/J.RSE.2016.09.014

Migliavacca, M., Galvagno, M., Cremonese, E., Rossini, M., Meroni, M., Sonnentag, O., … Richardson, A. D. (2011). Using digital repeat photography and eddy covariance data to model grassland phenology and photosynthetic CO 2 uptake. *Agricultural and Forest Meteorology*, *151*, 1325–1337. https://doi.org/10.1016/j.agrformet.2011.05.012

Munro, R. H. M., Nielsen, S. E., Price, M. H., Stenhouse, G. B., & Boyce, M. S. (2006). Seasonal and diel patterns of grizzly bear diet and activity in West-Central Alberta. *Journal of Mammalogy*, *87*(6), 1112–1121.

Nijland, W., Bolton, D. K., Coops, N. C., & Stenhouse, G. (2016). Remote sensing of environment imaging phenology; scaling from camera

plots to landscapes. *Remote Sensing of Environment*, *177*, 13–20. https://doi.org/10.1016/j.rse.2016.02.018

Nijland, W., Coops, N. C., Coogan, S. C. P., Bater, C. W., Wulder, M. A., Nielsen, S. E., … Stenhouse, G. B. (2013). Vegetation phenology can be captured with digital repeat photography and linked to variability of root nutrition in *Hedysarum Alpinum*. *Applied Vegetation Science*, *16*, 317–324. https://doi.org/10.1111/avsc.12000

Petitjean, F., Inglada, J., & Gançarski, P. (2012). Satellite image time series analysis under time warping. *IEEE Transactions on Geoscience and Remote Sensing*, *50*(8), 3081–3095. https://doi.org/10.1109/TGRS.2011.2179050

Plard, F., Gaillard, J.-M., Coulson, T., Hewison, A. J. M., Delorme, D., Warnant, C., & Bonenfant, C. (2014). Mismatch between birth date and vegetation phenology slows the demography of roe deer. *PLoS Biology*, *12*(4), 1001828. https://doi.org/10.1371/journal.pbio.1001828

R Core Team. (2018). *R: A language and environment for statistical computing*. Vienna, Austria: R Foundation for Statistical Computing. Retrieved from http://www.r-project.org/

Renner, S. S., & Zohner, C. M. (2018). Climate change and phenological mismatch in trophic interactions among plants, insects, and vertebrates. *Annual Review of Ecology, Evolution, and Systematics*, *49*(1), 165–182. https://doi.org/10.1146/annurev-ecolsys-110617-062535

Richardson, A. D., Hufkens, K., Milliman, T., Aubrecht, D. M., Chen, M., Gray, J. M., … Frolking, S. (2018). Tracking vegetation phenology across diverse North American biomes using PhenoCam imagery. *Scientific Data*, *5*, 180028. https://doi.org/10.1038/sdata.2018.28

Sakoe, H., & Chiba, S. (1978). Dynamic programming algorithm optimization for spoken word recognition. *IEEE Transactions on Acoustics, Speech, and Signal Processing*, *26*(1), 43–49. https://doi.org/10.1109/TASSP.1978.1163055

Schwartz, M. D. (Ed.). (2003). *Phenology: An integrative environmental science* (p. 564). Dordrecht, Netherlands: Kluwer Academic Publishers.

Schwartz, M. D., Ahas, R., & Aasa, A. (2006). Onset of spring starting earlier across the Northern Hemisphere. *Global Change Biology*, *12*(2), 343–351. https://doi.org/10.1111/j.1365-2486.2005.01097.x

Sonnentag, O., Hufkens, K., Teshera-Sterne, C., Young, A. M., Friedl, M., Braswell, B. H., … Richardson, A. D. (2012). Digital repeat photography for phenological research in forest ecosystems. *Agricultural and Forest Meteorology*, *152*, 159–177. https://doi.org/10.1016/J.AGRFORMET.2011.09.009

Soudani, K., Le Maire, G., Dufrêne, E., François, C., Delpierre, N., Ulrich, E., & Cecchini, S. (2008). Evaluation of the onset of green-up in temperate deciduous broadleaf forests derived from Moderate Resolution Imaging Spectroradiometer (MODIS) data. *Remote Sensing of Environment*, *112*(5), 2643–2655. https://doi.org/10.1016/J.RSE.2007.12.004

Uemura, S. (1994). Patterns of leaf phenology in forest understory. Retrieved from www.nrcresearchpress.com

Vartanian, M., Nijland, W., Coops, N. C., Bater, C., Wulder, M. A., & Stenhouse, G. (2014). Assessing the impact of field of view on monitoring understory and overstory phenology using digital repeat photography. *Canadian Journal of Remote Sensing*, *40*(2), 85–91. https://doi.org/10.1080/07038992.2014.930308

White, M. A., Hoffman, F., Hargrove, W. W., & Nemani, R. R. (2005). A global framework for monitoring phenological responses to climate change. *Geophysical Research Letters*, *32*(4), 1–4. https://doi.org/10.1029/2004GL021961

Wulder, M. A., Masek, J. G., Cohen, W. B., Loveland, T. R., & Woodcock, C. E. (2005). Opening the archive: How free data has enabled the science and monitoring promise of Landsat. *Remote Sensing of Environment*, *122*, 2–10. https://doi.org/10.1016/j.rse.2012.01.010

Zhang, X., Friedl, M. A., Schaaf, C. B., Strahler, A. H., Hodges, J. C. F., Gao, F., … Huete, A. (2003). Monitoring vegetation phenology using MODIS. *Remote Sensing of Environment*, *84*(3), 471–475. https://doi.org/10.1016/S0034-4257(02)00135-9

How to cite this article: McClelland CJR, Coops NC, Berman EE, et al. Detecting changes in understorey and canopy vegetation cycles in West Central Alberta using a fusion of Landsat and MODIS. *Appl Veg Sci*. 2020;23:223–238. https://doi.org/10.1111/avsc.12466